Section editor: Dr. M. Segal

Synaptic organization in $Ca_V1.3$ Ca^{2+} channel deficient cochlear hair cells

Rodrigue M. Nemzou N., Anna V. Bulankina, Darina Khimich, Alexander Giese and Tobias Moser

Department of Otolaryngology and Center for Molecular Physiology of the Brain, University of Göttingen, D-37099 Göttingen, Germany

Corresponding author:

Tobias Moser

Department of Otolaryngology and Center for Molecular Physiology of the Brain

University of Göttingen

D-37099 Göttingen, Germany

+49-551-398968

+49-551-3912950 (fax)

tmoser@gwdg.de

Abbreviations: IHC: inner hair cell; $Ca_V1.3$: α subunit 1.3 forming L-type voltage-gated Ca^{2+} channels; BK: large conductance calcium-activated potassium channel, *Kcnma1*: gene coding the large conductance calcium-activated potassium channel, subfamily M, α subunit 1; SK: small conductance Ca^{2+} activated K^+ channel; GluR: glutamate receptor; SGN: spiral ganglion neuron; NF-200: neurofilament of 200 kDa; CSP: cysteine string protein; RNA: ribonucleic acid; cDNA: complementary desoxyribonucleic acid; RT-PCR: reverse transcription + polymerase chain reaction; TBP: TATA-binding protein; 3D: three dimensional, 2D: two dimensional; GSDB: goat serum dilution buffer; PFA: paraformaldehyde.

Abstract

Cochlear inner hair cells (IHCs) release neurotransmitter onto afferent auditory nerve fibers in response to sound stimulation. Normal development and function of inner hair cells require the expression of $Ca_V1.3$ channels.

Here, we used immunohistochemistry and RT-PCR to study the synaptic organization and expression of large conductance Ca^{2+}-activated potassium channels in IHCs of mice lacking the $Ca_V1.3$ Ca^{2+} channel ($Ca_V1.3^{-/-}$). Despite the near complete block of evoked afferent synaptic transmission, hair cell ribbon synapses were formed and remained preserved for at least 4 weeks after birth. Moreover, these "silent" afferent synapses held major components of the synaptic machinery such as Bassoon, Piccolo, and CSP. Hence, the block of exocytosis might be solely attributed to the lack of Ca^{2+} influx through $Ca_V1.3$ channels. Later on, $Ca_V1.3$ deficient IHCs subsequently lost their afferent synapses. This was probably due to a secondary degeneration of the postsynaptic spiral ganglion neurons.

In line with a prolonged efferent synaptic transmission onto $Ca_V1.3$ deficient IHCs, which normally ceases around onset of hearing, we found juxtaposed immunoreactive spots of efferent presynaptic synaptophysin and postsynaptic (IHCs) small conductance Ca^{2+}-activated potassium channels (SK channels) up to six weeks after birth. Finally, we show a substantial reduction of messenger RNA for the α subunit of the large conductance Ca^{2+}-activated potassium channel (BK) in the apical cochlea, suggesting a reduced transcription of the *Kcnma1* gene in $Ca_V1.3$ deficient IHCs. $Ca_V1.3$ deficient IHCs lacked the apical spot-like immunoreactivity of clustered BK channels,

which normally contribute to the temporal precision of hair cell afferent synaptic transmission.

In summary, these data indicate that the $Ca_V1.3$ channels are crucially involved in regulation of the expression of BK and SK channels. $Ca_V1.3$ channels seem not to be essential for ribbon synapse formation, but are required for the maintenance of ribbon synapses and spiral ganglion neurons.

*Key words**: calcium channel, hair cell, ribbon synapse, synaptogenesis, efferent synapse, BK channel***

Inner hair cells (IHCs) are the genuine sensory cells of the mammalian cochlea that transmit mechanical stimuli into neuronal signals (Fuchs et al., 2003, Nouvian et al., 2006). About 95 % of the primary auditory neurons (type I spiral ganglion neurons) receive their input from IHCs using AMPA type glutamate receptors (Matsubara et al., 1996). Sound evoked gating of the IHC`s mechanotransducer channels causes a depolarizing receptor potential, which in turn activates basolateral voltage-gated Ca^{2+} and K^+ channels. In contrast to neuronal presynaptic terminals, IHC afferent synapses mainly contain L-type Ca^{2+}- channels, ~ 90% of which are $Ca_V1.3$ channels (Platzer et al., 2000, Brandt et al., 2003, Dou et al., 2004). These channels cluster at the active zones, where release of each fusion-competent synaptic vesicle is probably under Ca^{2+} nanodomain control exerted by one or few Ca^{2+} channels (Brandt et al., 2005).

Consequently, depolarization-evoked exocytosis is nearly abolished in $Ca_V1.3$ deficient IHCs (Brandt et al., 2003). However, robust exocytosis, as assayed by membrane capacitance measurements, could still be evoked when bypassing the lacking Ca^{2+} influx by intracellular release of Ca^{2+} using flash photolysis of caged Ca^{2+} (Brandt et al., 2003). It remained unclear, however, whether the block of depolarization-induced exocytosis in $Ca_V1.3$ deficient IHCs and the deafness included a more general defect of synaptic organization. In fact, a reduction of synaptic ribbons had been suggested for $Ca_V1.3$ deficient IHCs in a previous electron microscopy study (Glueckert et al., 2003). Hence, it remained possible that the preserved exocytosis evoked by Ca^{2+} uncaging was unrelated to synaptic transmission at ribbon synapses. In order to investigate ribbon synapse formation and to more quantitatively study the molecular anatomy of the afferent hair cell synapses in $Ca_V1.3$-deficient IHCs, we performed immunohistochemistry for

afferent synaptic markers at several developmental stages. This method has a high detection efficiency for ribbon-containing synapses, which are recognized as juxtaposed spots of presynaptic RIBEYE (ribbon marker, (Schmitz et al., 2000) and postsynaptic ionotropic glutamate receptor (GluR) immunofluorescence in 3 dimensional (3D) reconstructions of the organ of Corti (Khimich et al., 2005). In addition, it enables one to collect a large sample of synapses with moderate effort. In addition to RIBEYE we investigated the presence of key synaptic proteins Bassoon, Piccolo and CSP in the functionally "silent" $Ca_V1.3$ deficient IHCs.

Cochlear degeneration is the common final condition of many inner ear pathologies, including inherited cochlear dysfunction as well as toxic or noise damage to the cochlea. Eventually the failure or degeneration of the sensory cells leads to secondary loss of SGNs (Spoendlin, 1984). This has been mainly attributed to the loss of trophic support for SGNs by IHCs and supporting cells (Rubel and Fritzsch, 2002, Stankovic et al., 2004). The $Ca_V1.3$ mutant provided an excellent paradigm to specifically study the consequences of an IHC synaptic failure on the ascending auditory pathway, as IHCs are initially preserved (Platzer et al., 2000, Dou et al., 2004). Indeed, a loss of type I SGNs was observed in these mice (Glueckert et al., 2003). However, this previous study did not quantify the afferent fibers projecting to the "silent" IHCs, which may be reduced well before loss of the neuronal somata. Therefore, in addition to observing postsynaptic GluR clusters, we studied the abundance of afferent SGN fibers projecting towards $Ca_V1.3$-deficient IHCs.

Besides their impact on synaptic function, $Ca_V1.3$ channels seem to be essential for regulation of hair cell development. For example, the efferent synaptic control by

fibers of the medial olivocochlear bundle that is normally lost after the onset of hearing (Zuo et al., 1999, Glowatzki and Fuchs, 2000, Simmons, 2002, Brandt et al., 2003) seems to be maintained for several weeks in $Ca_V1.3^{-/-}$ mice (Brandt et al., 2003). At these cholinergic synapses unconventional ACh receptors formed from α9 and α10 subunits (Plazas et al., 2005) mediate a non-selective cation influx into IHCs. The incoming Ca^{2+} causes activation of small conductance Ca^{2+} activated potassium channels (SK channels; (Glowatzki and Fuchs, 2000, Oliver et al., 2000). The SK current results in a hyperpolarization of IHCs, which may interfere with the generation of Ca^{2+} action potentials (Glowatzki and Fuchs, 2000). While outer hair cells maintain efferent cholinergic inhibition throughout their life, IHCs loose the efferent inhibition during the second postnatal week (Katz et al., 2004). In order to explore the morphological basis of our previous physiological finding of prolonged efferent control of IHCs, we used immunohistochemistry to identify efferent hair cell synapses as juxtaposed spots of presynaptic synaptophysin and postsynaptic SK channels in control and $Ca_V1.3$ deficient IHCs at various developmental stages.

Furthermore, $Ca_V1.3$ channels are essential for the acquisition of fast outward currents mediated by large conductance Ca^{2+} activated potassium channels (BK channels) around the onset of hearing, which is another hallmark of normal IHC development (Kros et al., 1998). BK currents could not be observed in $Ca_V1.3$ deficient IHCs up to the fifth postnatal week (Brandt et al., 2003). It remained unclear, however, whether this was due to failure of transcription of the *Kcnma1* gene coding for the pore-forming α subunit of the BK channel, translation or targeting of normally synthesized protein to the plasma

membrane. Here, we performed RT-PCR and immunohistochemistry in order to address this question.

Experimental procedures

Solutions

The solution for explanting the organ of Corti (HEPES-Hank's) contained (in mM): 141 NaCl, 5.4 KCl, 1 $MgCl_2$, 0.5 $MgSO_4$, 6 L-Glutamine, 7 Glucose, and 10 NaOH-HEPES, pH 7.2. 120 mM Phosphate buffer contained: 100 mM Na_2HPO_4, 20 mM NaH_2PO_4. GSDB (goat serum dilution buffer) contained: 16% normal goat serum, 450 mM NaCl, 0.3% Triton X-100, 20 mM phosphate buffer, pH 7.4. Fixative contained either 4% paraformaldehyde (PFA) in 120 mM phosphate buffer, 99.9% Ethanol or 99.9% Methanol. Phosphate buffer saline contained (in mM): 140 NaCl, 2.7 KCl, 8 Na_2HPO_4, and 1.5 KH_2PO_4, pH 7.4. Wash buffer contained: 450 mM NaCl, 20 mM phosphate buffer, 0.3% Triton X-100.

Antibodies

The following antibodies were used: mouse anti-Bassoon Sap7f (diluted 1:1000-1:500, generated against amino acids 756-1001 of the Bassoon protein, gift of E. Gundelfinger, Magdeburg, Germany), guinea pig anti-Piccolo (1:1000, generated against amino acids 2172-2361 of Piccolo protein, (Fenster et al., 2000), gift of E.Gundelfinger, Magdeburg, Germany), Anti-CSP (1:400; Chemicon), Anti-CtBP2 mouse IgG1 (1:100-200; BD Biosciences; recognizing the B-domain of RIBEYE and the transcriptional co-repressor CtBP2 [c-terminal binding protein 2, hence both ribbons and nuclei are stained]; ribbon-staining overlapping with RIBEYE A-domain staining in IHCs, (Khimich et al., 2005), rabbit anti-glutamate receptors 2/3 affinity purified polyclonal antibody (1:300- 1:1000; Chemicon), mouse anti-parvalbumin235 monoclonal antibody (1:500; against

parvalbumin; Swant, Bellinzona, Switzerland), rabbit anti-parvalbumin28 (1:500, Swant), rabbit anti-BK_{Ca} channel (1:300; Alomone Labs, Jerusalem, Israel; recognizing the intracellular C-terminus of KCNMA1), mouse monoclonal anti-Neurofilament-200 (NF-200, 1:150-200, Sigma-Aldrich, St. Louis), rabbit anti-potassium channel SK2 (1:200; generated against amino acids 542-559 of potassium SK2 channel; Sigma-Aldrich, St. Louis), mouse monoclonal anti-Synaptophysin (1:400, Synaptic Systems, Goettingen, Germany), Alexa Fluor 568 (1:200, goat anti-rabbit IgG, Invitrogen), Alexa Fluor 568 (1:200, goat anti-mouse IgG, Invitrogen), Alexa Fluor 488 (1:200, goat anti-mouse IgG, Invitrogen), Alexa Fluor 488 (1:200, goat anti-guinea pig IgG, Invitrogen).
For Figure 4 C-D Hoechst 34850 (1:1000, nucleic acid stain, Invitrogen) was used to stain the nuclei in the organ of Corti.

Preparation of the organ of Corti

$Ca_V1.3^{-/-}$ mice (Platzer et al., 2000; kind gift of J. Striessnig, Innsbruck, Austria; mice were backcrossed for at least five generations into a C57BL/6N genetic background) or wild-type mice (wt) (C57BL/6N) of the specified age were killed by decapitation, according to national ethical guidelines. The scull was then sagitally cut into two parts that were placed into Petri dishes with ice-cooled HEPES-Hank's solution. Under the dissecting microscope, the brain was removed and the bulla was opened to expose the cochlea. The cochlea's bony envelope was carefully opened and the apical coil of the organ of Corti was removed with fine forceps. The stria vascularis of adult mice (more than 3 weeks old) usually attached to the bony capsule of the cochlea and was separated

from the organ of Corti along with the capsule. However, it frequently remained attached in preparations of the p6 organ of Corti and had to be carefully peeled off.

Immunostaining procedure

The freshly dissected apical cochlear turns were fixed with either 4% PFA for 1 hour on ice (standard), with 99.9% Ethanol (Merck) for 20 min at -20°C or with 99.9% Methanol (Merck) for 20 min at -20°C (where specified in figures and table legends). Thereafter the preparations were washed 3x10 min in phosphate buffer saline and incubated for 1 hour in GSDB in a wet chamber at room temperature. Primary antibodies were dissolved in GSDB buffer and applied overnight at +4°C in a wet chamber. After washing with wash buffer (3x10 min) the organs of Corti were incubated with secondary antibodies in GSDB in the wet light-protected chamber for 1 hour at room temperature. Then the preparations were washed 3x10 min in wash buffer and 1x10 min in 5 mM phosphate buffer, placed onto the glass microscope slides with a drop of fluorescence mounting medium (Dako A/S, Glostrup, Denmark) and covered with thin glass coverslips.

Confocal microscopy

Confocal images were acquired using a laser scanning confocal microscope LSM 510 (Carl Zeiss Jena, Germany) with 488 nm (Ar) and 543 nm (He-Ne) lasers for excitation. We used 40x oil or water immersion objectives and the bandpass filters 500-550 and 565-615 nm. To produce 3D reconstructions of the specimen a z-axis stack of 2D images was taken with a step size 0.2 μm. The pixel size was 0.09 x 0.09 μm.

For Figs. 4C-D we used a Leica TCS SP2 confocal microscope (Leica microsystems Heidelberg, Germany) with 405 nm (diode laser), 488 nm (Ar) and 546 nm (He-Ne) lasers for excitation, a 63x oil immersion objective and bandpass filters 410-485, 494-549 and 565-681 nm. To produce 3D reconstructions of the specimen a z-axis stack of 2D images was taken with a step size 0.32 μm. The pixel size was 0.07 x 0.07 μm.

Image analysis

Images were processed using LSM 510 software (Carl Zeiss Jena) or ImageJ and assembled for display in Adobe Photoshop and Illustrator software. Whole mount preparations of the organ of Corti provided the possibility to analyze several IHCs in a row. Juxtaposition of immunostained presynaptic ribbons and postsynaptic glutamate receptor clusters as well as of immunostained efferent presynaptic synaptophysin and postsynaptic SK2 was investigated in 3D reconstructions of the organ of Corti and accepted if there was no visually discernable space between the ribbon and the postsynapse in all three axes (Khimich et al., 2005). In order to quantitatively investigate the immunofluorescence data in organs of Corti of $Ca_V1.3$ deficient and wild-type mice, the number of all ribbons and ribbon-containing synapses, nerve fibers as well as of the SK2 spots juxtaposing synaptophysin immunofluorescence in the field of view were counted and divided by the number of observed IHCs. The number of IHCs in the field of view was estimated by counting CtBP2 stained nuclei (when PFA fixed) or parvalbumin-stained IHCs. Else, we relied on the average count of 5.2 ± 0.72 IHCs in the field of view (n = 21 observations on postnatal days 15, 30 and 100 using a 40x objective lens and 5x

optical zoom, with no major differences among the different ages). Quantitative data are presented as mean ± sem.

Single IHC RT-PCR and real-time RT-PCR

IHCs from the apical coils of freshly dissected organs of Corti were harvested after cleaning off supporting cells and at a high bath perfusion rate (3 ml/min). Each individual IHC was aspirated and the pipette content was expirated into first strand cDNA synthesis mix containing after the dilution 50mM Tris-HCl, pH 8.3, 75mM KCl, 5mM $MgCl_2$, 5mM DTT, 100 units of SuperScript™ II Reverse Transcriptase (Invitrogen) and 40 units RNaseOUT™ Ribonuclease inhibitor (Invitrogen). Reverse transcription was performed with oligo(dT)primers as described by the manufacturer. Aspirated bath solution was used as a negative control. Each cDNA mix was used as a template for two subsequent PCR reactions with nested primers specific for KCNMA1 and otoferlin (the IHC marker, Yasunaga et al., 1999) cDNA. Primer sequences are listed in Table 1.

For real-time RT-PCR we isolated total RNA from 8 apical cochlear turns per genotype for each experiment using TRIzol Reagent (Invitrogen). For the experiments on the whole cochlea, RNA was extracted from the two cochleae of each mouse for every experiment. Following the RT reaction with random hexamers (similar first strand cDNA synthesis mix as for single cell RT-PCR) cDNA was subjected to real-time PCR using ABI Prism 7000 Sequence Detection System (Applied Biosystems). cDNAs for KCNMA1, otoferlin and TBP (TATA-binding protein as a housekeeping gene) were selectively amplified (in triplicates) using commercially available TaqMan Gene Expression Assays (Mm00516078_m1, Mm00453306_m1 and Mm00446973_m1, Applied Biosystems) in separate reactions (20µl volume) according to the manufacturer protocol.

Relative amounts of KCNMA1 and otoferlin mRNAs, normalized to that of TBP, were calculated using the comparative $2^{-\Delta\Delta Ct}$ method (Applied Biosystems) and reported as mean ± sd. The slopes of the standard curves amounted to -3.56, -3.49 and -3.50 for KCNMA1, otoferlin and TBP, respectively.

Results

Ribbons and afferent dendrites are maintained up to 4 weeks and gradually lost thereafter in $Ca_V1.3$ deficient mice

We used immunostaining for RIBEYE/CtBP2 and GluR2/3 ionotropic glutamate receptors to visualize presynaptic ribbons and postsynaptic terminals, respectively (Khimich et al., 2005). Figure 1 shows representative projections obtained from z-stacks of confocal sections through apical cochlear turns of wild type and $Ca_V1.3$ deficient mice at different ages. Synaptic ribbons (red) were mostly juxtaposed to the postsynaptic GluR2/3 spots (green), probably representing ribbon-containing synapses also in $Ca_V1.3$ deficient IHCs. Specific postsynaptic staining was obtained better with ethanol fixation than with PFA fixation. Different from the staining pattern in IHCs of older mice (C-F and Khimich et al., 2005), the GluR2/3 immunoreactivity was not confined to sharply delimited spots with a one-to-one juxtaposition to a ribbon in immature IHCs (postnatal day 8 [p8], A, B). This might indicate that the clustering of ionotropic glutamate receptors undergoes maturation or reflect the presence of supernumerous postsynaptic terminals during synaptogenesis (Sobkowicz et al., 1982). As a result, there was a greater uncertainty in the light microscopical definition of a ribbon-containing synapse at this age. Hence, we only provide the total ribbon counts for p8, which were comparable among IHCs of mice of both genotypes (Fig.1 A, B; Table 2).

Around and early after the onset of hearing, the number of ribbon containing synapses was indistinguishable between IHCs of controls and mutants (Fig.1 C, D). However, we found a lower number of ribbon-containing synapses in IHCs of $Ca_V1.3^{-/-}$ mice starting from the second month (Fig.1 E, F). Both, presynaptic ribbons and

postsynaptic receptor clusters were equally affected. Table 2 summarizes the analysis for the different points in time. In the oldest mice analysed we found only ~ 3 ribbon-containing synapses per $Ca_V1.3$ deficient IHC, while no significant decrease was observed in the wild type IHCs after 4 weeks of age.

No obvious differences in the abundance of other key synaptic proteins (e.g. Bassoon and Piccolo) were observed among the two genotypes at 3 weeks of age by immunohistochemistry (Figure 2), while the synaptic co-chaperone CSP (Schmitz et al., 2006) was slightly less expressed.

In a separate set of experiments we visualized projections of spiral ganglion neurons to hair cells by co-staining for neurofilaments (NF-200, (Hafidi et al., 1990) and parvalbumin (Celio, 1990, Soto-Prior et al., 1995). Fibers were recognized by either staining, which in many cases overlapped. To a rough approximation of the number of type I SGN dendrites projecting to IHCs we counted NF-200 positive fibers approaching the hair cell zone in the field of view. Whereas the number of afferent fibers was only slightly reduced in organs of Corti of young $Ca_V1.3^{-/-}$ mice (Fig. 3A, B), a dramatic loss of fibers was observed in older animals (Fig. 3C, D and Table 2). In addition, a mild loss of IHCs was evident (e.g. Fig. 3D). Hence, both the numbers of ribbons and afferent fibers per IHC of $Ca_V1.3^{-/-}$ mice followed a similar declining trend over time.

Prolonged presence of efferent IHC synapses in $Ca_V1.3^{-/-}$ mice

We had previously reported postsynaptic currents to persist in IHCs of $Ca_V1.3^{-/-}$ mice up to at least p35 (Brandt et al., 2003). Seeking morphological evidence for a persistent efferent innervation of $Ca_V1.3^{-/-}$ IHCs we performed immunostaining for the efferent

presynaptic marker synaptophysin (absent from IHCs) and the small conductance Ca^{2+} activated potassium channel subtype SK2 (Fig. 4), which was shown to mediate the inhibitory signalling of efferent innervation in both IHCs (Katz et al., 2004) and outer hair cells (Oliver et al., 2000). Immature hair cells of each genotype showed efferent axosomatic synapses identified as juxtaposed pairs of presynaptic synaptophysin and postsynaptic SK2 immunofluorescent spots. To aid identification of the hair cell position we stained combined the immunolabeling with a nuclear staining in panels C and D. For quantification we relied on counting SK2 immunospots juxtaposing synaptophysin immunofluorescence (Table 2). Axosomatic synapses were still observed in $Ca_V1.3$ deficient IHCs in the fifth postnatal week (Fig.4F), albeit at lower number, while control IHCs were devoid of SK2 spots at this age. The synaptophysin immunoreactivity around the basolateral portion of the mature wild-type IHCs most likely represented efferent presynaptic terminals of the lateral olivocochlear bundle forming axodendritic synapses with afferent dendrites (Simmons, 2002).

Lack of BK-immunoreactivity and reduced abundance of the KCNMA1 mRNA in $Ca_V1.3^{-/-}$ IHCs

We had previously demonstrated a lack of BK currents in $Ca_V1.3^{-/-}$ IHCs even when depolarizing the cells in the intracellular presence of a high Ca^{2+} concentration (Brandt et al., 2003). This finding could in principle be due to defects of various cellular processes. Here we performed immunostaining for the BK channels in whole mounts of the organ of Corti to further address this question (Fig. 5A, B). Using an antibody directed against the BK channel alpha subunit 1 (KCNMA1) we observed the previously described apical,

spot-like BK immunoreactivity (Pyott et al., 2004) in all IHCs of 4-week-old control mice (A). However, we failed to detect specific BK signals in any IHC of $Ca_V1.3$ deficient mice at the same age (B).

Next, we tested for the abundance of KCNMA1 mRNA in $Ca_V1.3$ deficient IHCs at the end of the fourth postnatal week. Real-time RT-PCR on total RNA extracted from apical cochlear turns as well as single IHC RT-PCRs were performed (Fig. 5C-H). Otoferlin mRNA was detected as a control for sufficient IHC mRNA yield and TATA-binding protein (TBP) served as a reference. Real-time RT-PCR reported only a slight reduction of otoferlin mRNA in apical cochlear turns of $Ca_V1.3^{-/-}$ mice (88.3 ± 3.4% of $Ca_V1.3^{+/+}$, n = 5 for each genoytpe, 8 apical turns per experiment) indicating comparable numbers of IHCs at this age (in line with Figs. 1-3) and near normal abundance of otoferlin mRNA in mutant IHCs. The latter was supported by finding a comparable percentage of $Ca_V1.3^{+/+}$ (97 %) and $Ca_V1.3^{-/-}$ (96%) IHCs to be otoferlin-positive in the single cell RT-PCR (Fig. 5G, H). A total of 8 or 6 negative controls (including reverse transcriptase) and another 4 or 3 without reverse transcriptase were obtained for control and $Cav1.3^{-/-}$ animals, respectively.

At the same time real-time RT-PCR revealed a near twofold reduction of the KCNMA1 mRNA in apical cochlear turns of $Ca_V1.3^{-/-}$ mice (51.8 ± 2.6% of $Ca_V1.3^{+/+}$, n = 5 experiments for each genoytpe, 8 apical turns per experiment). A degenerative loss of OHCs has been shown in the apical cochlea of $Ca_V1.3^{-/-}$ mice already after ~ 2 weeks (Platzer et al., 2000; Glueckert et al., 2003, but see Dou et al., 2004 and discussion). Although apical OHCs show only low BK expression (Ruttiger et al., 2004), the reduction of the KCNMA1 mRNA observed in the apical cochlea $Ca_V1.3^{-/-}$ mice could be

partially due to the loss of apical OHCs. Therefore, we tested the abundance of KCNMA1 mRNA in total RNA extracted from the whole cochlea including the surviving basal OHCs (Dou et al., 2004) that express high levels of BK (Ruttiger et al., 2004). KCNMA1 mRNA was also reduced but to a lesser extent (to 72 ± 5.5 %, n = 3) while otoferlin mRNA was not significantly changed.

Next we specifically tested KCNMA1 mRNA abundance in IHCs using single-cell RT-PCR. While we detected the abundant otoferlin mRNA in nearly all cells tested in single-cell PCR (see above) we found KCNMA1 mRNA in only 77% of the $Ca_V1.3^{+/+}$ IHCs (24 out of 31). We (Brandt et al., 2003) and others (Kros and Crawford, 1990, Thurm et al., 2005) have obtained BK currents in each wild-type IHC investigated. Hence, we interpret this finding as a limited detection rate due to low KCNMA1 mRNA abundance. We consider that RNA degradation before the RT-reaction as well as incomplete sampling of IHC content contribute to underestimation of mRNA abundance, which in some cases results in a negative RT-PCR result for KCNMA1. Likewise, we take the even lower fraction of KCNMA1 positive IHCs in $Ca_V1.3^{-/-}$ mice IHCs (H, 26 %, 6 out of 23) to indicate a reduced KCNMA1 mRNA abundance in $Ca_V1.3^{-/-}$ IHCs, hence, supporting our real-time PCR finding.

Discussion

In this study we investigated the formation and maintenance of synaptic structures in auditory hair cells that largely lack synaptic activity due to inactivation of the gene coding for the $Ca_V1.3$ Ca^{2+} channel. The $Ca_V1.3$ channel is not only the key element of hair cell stimulus-secretion coupling (Brandt et al., 2003; Brandt et al., 2005) but also mediates the pre-sensory regenerative Ca^{2+} signaling (Kros et al., 1998; Glowatzki and Fuchs, 2000; (Beutner and Moser, 2001); Brandt et al., 2003) that might be linked to hair cell specific gene expression. The present results show that formation of hair cell ribbon synapses does not depend on either role of the $Ca_V1.3$ channel. However, synapses, postsynaptic SGNs and finally IHCs are slowly lost probably due to the prolonged absence of evoked synaptic activity. In addition, two major failures of IHC development - prolonged persistence of efferent cholinergic synapses and reduced abundance of KCNMA1 mRNA - were observed, probably resulting from the lack of afferent synaptic activity and neonatal Ca^{2+} action potential firing.

Formation and maintenance of hair cell synapses

Afferent synapses of IHCs are already present in newborn mice (Shnerson et al., 1981); (Sobkowicz et al., 1982). Synapse formation requires functional chemotactic and neurotrophic signaling (Fritzsch and Rubel, 2002). During the first postnatal week a peak of IHC synaptogenesis has been observed by electron microscopy (Sobkowitz et al., 1982), which goes along with a peak of Ca^{2+} current density (Beutner and Moser, 2001, Brandt et al., 2003, Johnson et al., 2005) and robust pre-sensory transmitter release from IHCs (Beutner and Moser, 2001, Glowatzki and Fuchs, 2002, Johnson et al., 2005).

Morphologically, this stage is characterized by large active zones anchoring multiple ribbons (Sobkowitz et al., 1982) and by branching afferent fibers (Echteler, 1992) with each of the branches capable of forming multiple synaptic contacts (Sobkowitz et al., 1982). Our confocal analysis of RIBEYE immunolabelling could not discriminate single from multiple ribbons, hence, our immunohistochemistry-based ribbon count is likely to be an underestimate. We refrained from estimating the number of anchored ribbons based on confocal analysis at this stage, because the immunofluorescence obtained with the GluR2/3 antibody [which probably reflects the sole presence of GluR3, as GluR2 is not yet expressed (Eybalin et al., 2004)] was very particular at this developmental stage but comparable in both genotypes (Figure 1A-B). Different from the mature situation, we found smaller and partially confluent GluR2/3 immunospots, which clearly exceeded the RIBEYE spots in number. Therefore, although most RIBEYE spots juxtaposed GluR2/3 immunofluorescence, we cannot be sure that they represent proper ribbon synapses. A similar immunofluorescence pattern was observed when staining immature, wild-type organs of Corti using an antibody against GluR4, arguing against a GluR3 specific distribution pattern (data not shown). GluR2/3 spots devoid of juxtaposed RIBEYE fluorescence may indicate nascent afferent synapses and/or zones of glutamate receptor assembly that later form larger clusters at synapses. To our knowledge, a prominent abundance of ribbon-lacking synaptic contacts with clearly discernible postsynaptic densities has not been described in previous electron microscopy studies of the developing organ of Corti. This could suggest that the ribbon-lacking glutamate receptor clusters observed in the present study might not reside in proper postsynaptic densities and may not represent mature receptor assemblies. It seems likely that these numerous

GluR2/3 spots reflect the large number of dendritic branches that later on are lost by pruning (Echteler, 1992). It remains to be tested, to which extent such clusters might contribute to excitatory postsynaptic currents in immature organs of Corti (Glowatzki and Fuchs, 2002).

Around and after the onset of hearing IHCs of control and $Ca_V1.3^{-/-}$ mice showed comparable synapse numbers. This remained true until the fourth postnatal week. The postsynaptic GluR2/3 staining in $Ca_V1.3^{-/-}$ mice adopted the normal, mature appearance of sharply delimited spots, which were strictly juxtaposed to presynaptic ribbons. Hence the main conclusion is that ribbon synapses are formed and remain undistinguishable from control synapses at the light-microscopy level up to four weeks. The latter suggests that at least some ribbon dynamics is at work.

Besides, mutant IHCs also expressed important synaptic genes: CSP, Bassoon, Piccolo and otoferlin. This indicates that $Ca_V1.3$ deficient IHC synapses achieve much of their normal molecular make-up and morphology and argues against a general synaptic defect. Hence, our previous physiological finding of maintained flash-photolysis-induced exocytosis in mutant IHCs at 2-4 weeks of age can, most likely, be taken to represent release of synaptic vesicles at and probably also outside ribbon-containing active zones. Afferent synaptogenesis despite the block of evoked transmitter release is reminiscent of the observation of synapse formation in mice lacking key synaptic proteins, such as munc18-1 (Verhage et al., 2000) or SNAP-25 (Molnar et al., 2002). This provides further support for the view that activity-independent cues are sufficient for basic aspects of synaptogenesis.

We initially expected to observe a major degeneration of afferent synapses of $Ca_V1.3$-deficient IHCs at the end of the second week. Postsynaptic signs of degeneration had been described by electron microscopy as early as on p7 (Platzer et al., 2000, Glueckert et al., 2003) and the number of ribbons was suggested to decline starting from p3. Hence, the finding of a normal number of hair ribbon synapses in young and of residual ribbons in 6-month-old $Ca_V1.3$ deficient mice came as a surprise. The previous report probably represents an underestimate, because the small IHC ribbons can easily escape detection in random sections in electron microscopy (a note of caution about this problem had been added by these authors; see also Khimich et al., 2005; (Francis et al., 2005). In addition, both RIBEYE and GluR2/3 immunospots are lost simultaneously in organs of Corti of $Ca_V1.3^{-/-}$ mice, which is in contrast to Bassoon mutants that maintain the postsynaptic GluR2/3 spots. Hence, the $Ca_V1.3$ knockout should not be considered a prime model to study the effects of hair cell ribbon deficiency.

Developmental failure of IHCs lacking $Ca_V1.3$ channels

In contrast to afferent synaptogenesis and synapse elimination during postnatal development, the loss of efferent IHC synapses and the expression of the *Kcnma1* gene in IHCs around the onset of hearing were directly or indirectly affected by the lack of $Ca_V1.3$ channels. The transient cholinergic inhibition exerted by fibers of the medial olivocochlear bundle was suggested to inhibit regenerative Ca^{2+} signaling of neonatal IHCs (Glowatzki and Fuchs, 2000). These Ca^{2+} action potentials (Kros et al., 1998) drive hair cell transmitter release (Beutner and Moser, 2001; Glowatzki and Fuchs, 2002; Johnson et al., 2005) before the onset of hearing *in vitro*. Around the onset of hearing

action potentials but also efferent innervation are lost in normal IHCs (Glowatzki and Fuchs, 2000; Brandt et al., 2003; Katz et al., 2004). The present finding of juxtaposed synaptophysin and SK2 immunoreactive spots around the IHC membrane provides a molecular and morphological confirmation of our previous electrophysiological observation of persistent efferent control of IHCs in $Ca_V1.3$ knockout mice (Brandt et al., 2003). It is tempting to speculate, that the lack of sound-driven transmitter release in $Ca_V1.3$ deficient IHCs may cause the maintenance of efferent hair cell innervation. It remains unclear, whether the lack of afferent input causes the efferent neurons of the superior olive to maintain their contact with the IHCs, a persistent postsynaptic signal of the hair cells primarily ensures the synaptic contact or yet another mechanism is at work.

Another hallmark of impaired IHC development in $Ca_V1.3$ knockout mice is the absence of BK current up to 4 weeks after birth (Brandt et al., 2003). Immunohistochemistry was used to distinguish a potential lack or miss-sorting of KCNMA1 channel protein from a functional defect despite correct membrane targeting. KCNMA1 immunoreactivity was readily detected at the neck of wild type hair cells as previously described (Pyott et al., 2004)et al., 2005). Hence, BK channels mostly localize remote from ribbon synapses where $Ca_V1.3$ channels cluster (Brandt et al., 2005). This readily explains why manipulations of voltage gated Ca^{2+} influx have little effect on the BK current in IHCs (Marcotti et al., 2004, Thurm et al., 2005). The lack of BK immunoreactivity in $Ca_V1.3$ deficient IHCs is in full agreement with our previous patch-clamp experiments, which also involved recordings at elevated cytosolic Ca^{2+} concentration (Brandt et al., 2003), and most likely reflects the absence of the channel from the plasma membrane. Even though the negative immunostaining could have

resulted from impaired clustering and hence a diffuse presence of the channel in the plasma membrane, BK currents should still have been observed.

Real-time RT-PCR performed during the 4th postnatal week showed a reduction of KCNMA1 mRNA in apical cochlear coils and whole cochleae of $Ca_V1.3$ deficient mice. Interpretation of this result could be complicated by degenerative loss of OHCs, which also express BK channels (Langer et al., 2003), albeit at lower level than IHCs and with a basoapical gradient (lowest expression in apex: Ruttiger et al., 2004). Previous studies on in $Ca_V1.3$ deficient mice have reported a sporadic loss of apical OHCs already at p15 {Platzer et al., 2000; Glueckert et al., 2003), while others found much less and slower degeneration of apical OHCs in their detailed histological analysis (Dou et al., 2004). In our sample, we found moderate to severe loss of OHCs in $Ca_V1.3^{-/-}$ mice at the age at which the real-time PCR was performed. The results of single IHC RT-PCR and real-time PCR on both the apical cochlear turn and the whole cochlea together with the low levels of BK expression (Ruttiger, 2004) in apical OHCs lead us to conclude that, indeed, KCNMA1 mRNA is less abundant in $Ca_V1.3^{-/-}$ IHCs.

How the lack of $Ca_V1.3$ channels causes the reduction of KCNMA1 mRNA remains to be established. We would like to speculate that the neonatal regenerative Ca^{2+} signaling mediated by $Ca_V1.3$ dependent action potentials contributes to regulation of postnatal IHC differentiation that includes enhanced transcription of the *Kcnma1* gene. The reduced levels of KCNMA1 mRNA might not provide for sufficient production of BK channels α subunits. Alternative mechanisms include enhanced degradation of KCNMA1 mRNA, inhibition of translation as well as miss-sorting and rapid degradation of KCNMA1.

Clinical implications

The $Ca_V1.3$ knockout mouse model with its loss of ribbon synapses, afferent dendrites (this study) and SGN (Glueckert et al., 2003) illustrates the consequences of a hair cell synaptopathy for the peripheral auditory system and potential therapeutic interventions. The two studies report a comparable time course of afferent dendrite and spiral ganglion cell loss (reduction to about 50 % within ~ 8 weeks after birth) in $Ca_V1.3$ knockout mice. If the results obtained from this animal model of impaired hair cell transmitter release can be transferred to human disease, the conclusion is that there is only a limited amount of time that can pass before cochlear implantation and electrical stimulation of spiral ganglion neurons, which then can support their survival (review in (Roehm and Hansen, 2005). The same applies for any future gene therapy. However, the decline takes longer than one might have thought for a near complete functional block of afferent synaptic transmission. In addition, the $Ca_V1.3$ mutant provides an interesting model system to study the central auditory systems changes to peripheral functional auditory deprivation.

Acknowledgements

Immunohistochemistry was performed by R. N. with some contribution of D.K., PCR by A.B. with some contribution of D.K. We would like to thank J. Striessnig for providing $Ca_V1.3$ knockout mice, A. Neef for help with the statistics on real-time PCR results, I. Roux for providing primer sequences for otoferlin, and S. Sigrist, E. Ponimaskin and K. Glebov for help with real-time PCR, A. Neef and R. Nouvian for discussion and their comments on the manuscript and M. Köppler as well as A. Gonzalez for excellent technical assistance. This work

was supported by the DFG (through the DFG Research Center for Molecular Physiology of the Brain [CMPB]), a Human Frontiers Science Program grant and an EC grant (EuroHear) to T.M.

References

Beutner, D. and Moser, T., 2001. The presynaptic function of mouse cochlear inner hair cells during development of hearing. J Neurosci. 21, 4593-4599.

Brandt, A., Khimich, D. and Moser, T., 2005. Few CaV1.3 channels regulate the exocytosis of a synaptic vesicle at the hair cell ribbon synapse. J Neurosci. 25, 11577-11585.

Brandt, A., Striessnig, J. and Moser, T., 2003. CaV1.3 channels are essential for development and presynaptic activity of cochlear inner hair cells. J Neurosci. 23, 10832-10840.

Celio, M. R., 1990. Calbindin D-28k and parvalbumin in the rat nervous system. Neuroscience. 35, 375-475.

Dou, H., Vazquez, A. E., Namkung, Y., Chu, H., Cardell, E. L., Nie, L., Parson, S., Shin, H. S. and Yamoah, E. N., 2004. Null mutation of alpha1D Ca2+ channel gene results in deafness but no vestibular defect in mice. J Assoc Res Otolaryngol. 5, 215-226.

Echteler, S. M., 1992. Developmental segregation in the afferent projections to mammalian auditory hair cells. Proc Natl Acad Sci U S A. 89, 6324-6327.

Eybalin, M., Caicedo, A., Renard, N., Ruel, J. and Puel, J. L., 2004. Transient Ca2+-permeable AMPA receptors in postnatal rat primary auditory neurons. Eur J Neurosci. 20, 2981-2989.

Fenster, S. D., Chung, W. J., Zhai, R., Cases-Langhoff, C., Voss, B., Garner, A. M., Kaempf, U., Kindler, S., Gundelfinger, E. D. and Garner, C. C., 2000. Piccolo, a presynaptic zinc finger protein structurally related to bassoon. Neuron. 25, 203-214.

Francis, H. W., Rivas, A., Lehar, M., Saito, Y., Mouton, P. R. and Ryugo, D. K., 2005. Efficient quantification of afferent cochlear ultrastructure using design-based stereology. J Neurosci Methods.

Fuchs, P. A., Glowatzki, E. and Moser, T., 2003. The afferent synapse of cochlear hair cells. Curr Opin Neurobiol. 13, 452-458.

Glowatzki, E. and Fuchs, P. A., 2000. Cholinergic synaptic inhibition of inner hair cells in the neonatal mammalian cochlea. Science. 288, 2366-2368.

Glowatzki, E. and Fuchs, P. A., 2002. Transmitter release at the hair cell ribbon synapse. Nat Neurosci. 5, 147-154.

Glueckert, R., Wietzorrek, G., Kammen-Jolly, K., Scholtz, A., Stephan, K., Striessnig, J. and Schrott-Fischer, A., 2003. Role of class D L-type Ca(2+) channels for cochlear morphology. Hear Res. 178, 95-105.

Hafidi, A., Despres, G. and Romand, R., 1990. Cochlear innervation in the developing rat: an immunocytochemical study of neurofilament and spectrin proteins. J Comp Neurol. 300, 153-161.

Hafidi, A., Beurg, M. and Dulon, D., 2005. Localization and developmental expression of BK channels in mammalian cochlear hair cells. Neuroscience. 130, 475-484.
Johnson, S. L., Marcotti, W. and Kros, C. J., 2005. Increase in efficiency and reduction in Ca2+ dependence of exocytosis during development of mouse inner hair cells. J Physiol. 563, 177-191.
Katz, E., Elgoyhen, A. B., Gomez-Casati, M. E., Knipper, M., Vetter, D. E., Fuchs, P. A. and Glowatzki, E., 2004. Developmental regulation of nicotinic synapses on cochlear inner hair cells. J Neurosci. 24, 7814-7820.
Khimich, D., Nouvian, R., Pujol, R., Tom Dieck, S., Egner, A., Gundelfinger, E. D. and Moser, T., 2005. Hair cell synaptic ribbons are essential for synchronous auditory signalling. Nature. 434, 889-894.
Kros, C. J., Ruppersberg, J. P. and Rusch, A., 1998. Expression of a potassium current in inner hair cells during development of hearing in mice. Nature. 394, 281-284.
Langer, P., Grunder, S. and Rusch, A., 2003. Expression of Ca2+-activated BK channel mRNA and its splice variants in the rat cochlea. J Comp Neurol. 455, 198-209.
Lioudyno, M., Hiel, H., Kong, J. H., Katz, E., Waldman, E., Parameshwaran-Iyer, S., Glowatzki, E. and Fuchs, P. A., 2004. A "synaptoplasmic cistern" mediates rapid inhibition of cochlear hair cells. J Neurosci. 24, 11160-11164.
Marcotti, W., Johnson, S. L. and Kros, C. J., 2004. Effects of intracellular stores and extracellular Ca(2+) on Ca(2+)-activated K(+) currents in mature mouse inner hair cells. J Physiol. 557, 613-633.
Matsubara, A., Laake, J. H., Davanger, S., Usami, S. and Ottersen, O. P., 1996. Organization of AMPA receptor subunits at a glutamate synapse: a quantitative immunogold analysis of hair cell synapses in the rat organ of Corti. J Neurosci. 16, 4457-4467.
Molnar, Z., Lopez-Bendito, G., Small, J., Partridge, L. D., Blakemore, C. and Wilson, M. C., 2002. Normal development of embryonic thalamocortical connectivity in the absence of evoked synaptic activity. J Neurosci. 22, 10313-10323.
Oliver, D., Klocker, N., Schuck, J., Baukrowitz, T., Ruppersberg, J. P. and Fakler, B., 2000. Gating of Ca2+-activated K+ channels controls fast inhibitory synaptic transmission at auditory outer hair cells. Neuron. 26, 595-601.
Platzer, J., Engel, J., Schrott-Fischer, A., Stephan, K., Bova, S., Chen, H., Zheng, H. and Striessnig, J., 2000. Congenital deafness and sinoatrial node dysfunction in mice lacking class D L-type Ca2+ channels. Cell. 102, 89-97.
Plazas, P. V., Katz, E., Gomez-Casati, M. E., Bouzat, C. and Elgoyhen, A. B., 2005. Stoichiometry of the alpha9alpha10 nicotinic cholinergic receptor. J Neurosci. 25, 10905-10912.
Pyott, S. J., Glowatzki, E., Trimmer, J. S. and Aldrich, R. W., 2004. Extrasynaptic localization of inactivating calcium-activated potassium channels in mouse inner hair cells. J Neurosci. 24, 9469-9474.
Roehm, P. C. and Hansen, M. R., 2005. Strategies to preserve or regenerate spiral ganglion neurons. Curr Opin Otolaryngol Head Neck Surg. 13, 294-300.
Rubel, E. W. and Fritzsch, B., 2002. Auditory system development: primary auditory neurons and their targets. Annu Rev Neurosci. 25, 51-101.
Ruttiger, L., Sausbier, M., Zimmermann, U., Winter, H., Braig, C., Engel, J., Knirsch, M., Arntz, C., Langer, P., Hirt, B., Muller, M., Kopschall, I., Pfister, M.,

Munkner, S., Rohbock, K., Pfaff, I., Rusch, A., Ruth, P. and Knipper, M., 2004. Deletion of the Ca2+-activated potassium (BK) alpha-subunit but not the BKbeta1-subunit leads to progressive hearing loss. Proc Natl Acad Sci U S A. 101, 12922-12927.

Schmitz, F., Konigstorfer, A. and Sudhof, T. C., 2000. RIBEYE, a component of synaptic ribbons: a protein's journey through evolution provides insight into synaptic ribbon function. Neuron. 28, 857-872.

Beutner, D. and Moser, T., 2001. The presynaptic function of mouse cochlear inner hair cells during development of hearing. J Neurosci. 21, 4593-4599.

Brandt, A., Khimich, D. and Moser, T., 2005. Few CaV1.3 channels regulate the exocytosis of a synaptic vesicle at the hair cell ribbon synapse. J Neurosci. 25, 11577-11585.

Brandt, A., Striessnig, J. and Moser, T., 2003. CaV1.3 channels are essential for development and presynaptic activity of cochlear inner hair cells. J Neurosci. 23, 10832-10840.

Celio, M. R., 1990. Calbindin D-28k and parvalbumin in the rat nervous system. Neuroscience. 35, 375-475.

Dou, H., Vazquez, A. E., Namkung, Y., Chu, H., Cardell, E. L., Nie, L., Parson, S., Shin, H. S. and Yamoah, E. N., 2004. Null mutation of alpha1D Ca2+ channel gene results in deafness but no vestibular defect in mice. J Assoc Res Otolaryngol. 5, 215-226.

Echteler, S. M., 1992. Developmental segregation in the afferent projections to mammalian auditory hair cells. Proc Natl Acad Sci U S A. 89, 6324-6327.

Eybalin, M., Caicedo, A., Renard, N., Ruel, J. and Puel, J. L., 2004. Transient Ca2+-permeable AMPA receptors in postnatal rat primary auditory neurons. Eur J Neurosci. 20, 2981-2989.

Fenster, S. D., Chung, W. J., Zhai, R., Cases-Langhoff, C., Voss, B., Garner, A. M., Kaempf, U., Kindler, S., Gundelfinger, E. D. and Garner, C. C., 2000. Piccolo, a presynaptic zinc finger protein structurally related to bassoon. Neuron. 25, 203-214.

Francis, H. W., Rivas, A., Lehar, M., Saito, Y., Mouton, P. R. and Ryugo, D. K., 2005. Efficient quantification of afferent cochlear ultrastructure using design-based stereology. J Neurosci Methods.

Fuchs, P. A., Glowatzki, E. and Moser, T., 2003. The afferent synapse of cochlear hair cells. Curr Opin Neurobiol. 13, 452-458.

Glowatzki, E. and Fuchs, P. A., 2000. Cholinergic synaptic inhibition of inner hair cells in the neonatal mammalian cochlea. Science. 288, 2366-2368.

Glowatzki, E. and Fuchs, P. A., 2002. Transmitter release at the hair cell ribbon synapse. Nat Neurosci. 5, 147-154.

Glueckert, R., Wietzorrek, G., Kammen-Jolly, K., Scholtz, A., Stephan, K., Striessnig, J. and Schrott-Fischer, A., 2003. Role of class D L-type Ca(2+) channels for cochlear morphology. Hear Res. 178, 95-105.

Hafidi, A., Despres, G. and Romand, R., 1990. Cochlear innervation in the developing rat: an immunocytochemical study of neurofilament and spectrin proteins. J Comp Neurol. 300, 153-161.

Johnson, S. L., Marcotti, W. and Kros, C. J., 2005. Increase in efficiency and reduction in Ca2+ dependence of exocytosis during development of mouse inner hair cells. J Physiol. 563, 177-191.
Katz, E., Elgoyhen, A. B., Gomez-Casati, M. E., Knipper, M., Vetter, D. E., Fuchs, P. A. and Glowatzki, E., 2004. Developmental regulation of nicotinic synapses on cochlear inner hair cells. J Neurosci. 24, 7814-7820.
Khimich, D., Nouvian, R., Pujol, R., Tom Dieck, S., Egner, A., Gundelfinger, E. D. and Moser, T., 2005. Hair cell synaptic ribbons are essential for synchronous auditory signalling. Nature. 434, 889-894.
Kros, C. J. and Crawford, A. C., 1990. Potassium currents in inner hair cells isolated from the guinea-pig cochlea. J Physiol. 421, 263-291.
Kros, C. J., Ruppersberg, J. P. and Rusch, A., 1998. Expression of a potassium current in inner hair cells during development of hearing in mice. Nature. 394, 281-284.
Marcotti, W., Johnson, S. L. and Kros, C. J., 2004. Effects of intracellular stores and extracellular Ca(2+) on Ca(2+)-activated K(+) currents in mature mouse inner hair cells. J Physiol. 557, 613-633.
Matsubara, A., Laake, J. H., Davanger, S., Usami, S. and Ottersen, O. P., 1996. Organization of AMPA receptor subunits at a glutamate synapse: a quantitative immunogold analysis of hair cell synapses in the rat organ of Corti. J Neurosci. 16, 4457-4467.
Molnar, Z., Lopez-Bendito, G., Small, J., Partridge, L. D., Blakemore, C. and Wilson, M. C., 2002. Normal development of embryonic thalamocortical connectivity in the absence of evoked synaptic activity. J Neurosci. 22, 10313-10323.
Nouvian, R., Beutner, D., Parsons, T. D. and Moser, T., 2006. Structure and function of the hair cell ribbon synapse. J Membr Biol. 209, 153-165.
Oliver, D., Klocker, N., Schuck, J., Baukrowitz, T., Ruppersberg, J. P. and Fakler, B., 2000. Gating of Ca2+-activated K+ channels controls fast inhibitory synaptic transmission at auditory outer hair cells. Neuron. 26, 595-601.
Platzer, J., Engel, J., Schrott-Fischer, A., Stephan, K., Bova, S., Chen, H., Zheng, H. and Striessnig, J., 2000. Congenital deafness and sinoatrial node dysfunction in mice lacking class D L-type Ca2+ channels. Cell. 102, 89-97.
Plazas, P. V., Katz, E., Gomez-Casati, M. E., Bouzat, C. and Elgoyhen, A. B., 2005. Stoichiometry of the alpha9alpha10 nicotinic cholinergic receptor. J Neurosci. 25, 10905-10912.
Pyott, S. J., Glowatzki, E., Trimmer, J. S. and Aldrich, R. W., 2004. Extrasynaptic localization of inactivating calcium-activated potassium channels in mouse inner hair cells. J Neurosci. 24, 9469-9474.
Roehm, P. C. and Hansen, M. R., 2005. Strategies to preserve or regenerate spiral ganglion neurons. Curr Opin Otolaryngol Head Neck Surg. 13, 294-300.
Rubel, E. W. and Fritzsch, B., 2002. Auditory system development: primary auditory neurons and their targets. Annu Rev Neurosci. 25, 51-101.
Schmitz, F., Konigstorfer, A. and Sudhof, T. C., 2000. RIBEYE, a component of synaptic ribbons: a protein's journey through evolution provides insight into synaptic ribbon function. Neuron. 28, 857-872.
Shnerson, A., Devigne, C. and Pujol, R., 1981. Age-related changes in the C57BL/6J mouse cochlea. II. Ultrastructural findings. Brain Res. 254, 77-88.

Simmons, D. D., 2002. Development of the inner ear efferent system across vertebrate species. J Neurobiol. 53, 228-250.
Sobkowicz, H. M., Rose, J. E., Scott, G. E. and Slapnick, S. M., 1982. Ribbon synapses in the developing intact and cultured organ of Corti in the mouse. J Neurosci. 2, 942-957.
Soto-Prior, A., Cluzel, M., Renard, N., Ripoll, C., Lavigne-Rebillard, M., Eybalin, M. and Hamel, C. P., 1995. Molecular cloning and expression of alpha parvalbumin in the guinea pig cochlea. Brain Res Mol Brain Res. 34, 337-342.
Spoendlin, H., 1984. Factors inducing retrograde degeneration of the cochlear nerve. Ann Otol Rhinol Laryngol Suppl. 112, 76-82.
Stankovic, K., Rio, C., Xia, A., Sugawara, M., Adams, J. C., Liberman, M. C. and Corfas, G., 2004. Survival of adult spiral ganglion neurons requires erbB receptor signaling in the inner ear. J Neurosci. 24, 8651-8661.
Thurm, H., Fakler, B. and Oliver, D., 2005. Ca2+-independent activation of BKCa channels at negative potentials in mammalian inner hair cells. J Physiol. 569, 137-151.
Verhage, M., Maia, A. S., Plomp, J. J., Brussaard, A. B., Heeroma, J. H., Vermeer, H., Toonen, R. F., Hammer, R. E., van den Berg, T. K., Missler, M., Geuze, H. J. and Sudhof, T. C., 2000. Synaptic assembly of the brain in the absence of neurotransmitter secretion. Science. 287, 864-869.
Zuo, J., Treadaway, J., Buckner, T. W. and Fritzsch, B., 1999. Visualization of alpha9 acetylcholine receptor expression in hair cells of transgenic mice containing a modified bacterial artificial chromosome. Proc Natl Acad Sci U S A. 96, 14100-14105.
Shnerson, A., Devigne, C. and Pujol, R., 1981. Age-related changes in the C57BL/6J mouse cochlea. II. Ultrastructural findings. Brain Res. 254, 77-88.
Simmons, D. D., 2002. Development of the inner ear efferent system across vertebrate species. J Neurobiol. 53, 228-250.
Sobkowicz, H. M., Rose, J. E., Scott, G. E. and Slapnick, S. M., 1982. Ribbon synapses in the developing intact and cultured organ of Corti in the mouse. J Neurosci. 2, 942-957.
Soto-Prior, A., Cluzel, M., Renard, N., Ripoll, C., Lavigne-Rebillard, M., Eybalin, M. and Hamel, C. P., 1995. Molecular cloning and expression of alpha parvalbumin in the guinea pig cochlea. Brain Res Mol Brain Res. 34, 337-342.
Spoendlin, H., 1984. Factors inducing retrograde degeneration of the cochlear nerve. Ann Otol Rhinol Laryngol Suppl. 112, 76-82.
Stankovic, K., Rio, C., Xia, A., Sugawara, M., Adams, J. C., Liberman, M. C. and Corfas, G., 2004. Survival of adult spiral ganglion neurons requires erbB receptor signaling in the inner ear. J Neurosci. 24, 8651-8661.
Thurm, H., Fakler, B. and Oliver, D., 2005. Ca2+-independent activation of BKCa channels at negative potentials in mammalian inner hair cells. J Physiol. 569, 137-151.
Verhage, M., Maia, A. S., Plomp, J. J., Brussaard, A. B., Heeroma, J. H., Vermeer, H., Toonen, R. F., Hammer, R. E., van den Berg, T. K., Missler, M., Geuze, H. J. and Sudhof, T. C., 2000. Synaptic assembly of the brain in the absence of neurotransmitter secretion. Science. 287, 864-869.

Yasunaga, S., Grati, M., Cohen-Salmon, M., El-Amraoui, A., Mustapha, M., Salem, N., El-Zir, E., Loiselet, J. and Petit, C., 1999. A mutation in OTOF, encoding otoferlin, a FER-1-like protein, causes DFNB9, a nonsyndromic form of deafness. Nat Genet. 21, 363-369.

Zuo, J., Treadaway, J., Buckner, T. W. and Fritzsch, B., 1999. Visualization of alpha9 acetylcholine receptor expression in hair cells of transgenic mice containing a modified bacterial artificial chromosome. Proc Natl Acad Sci U S A. 96, 14100-14105.

Figure legends

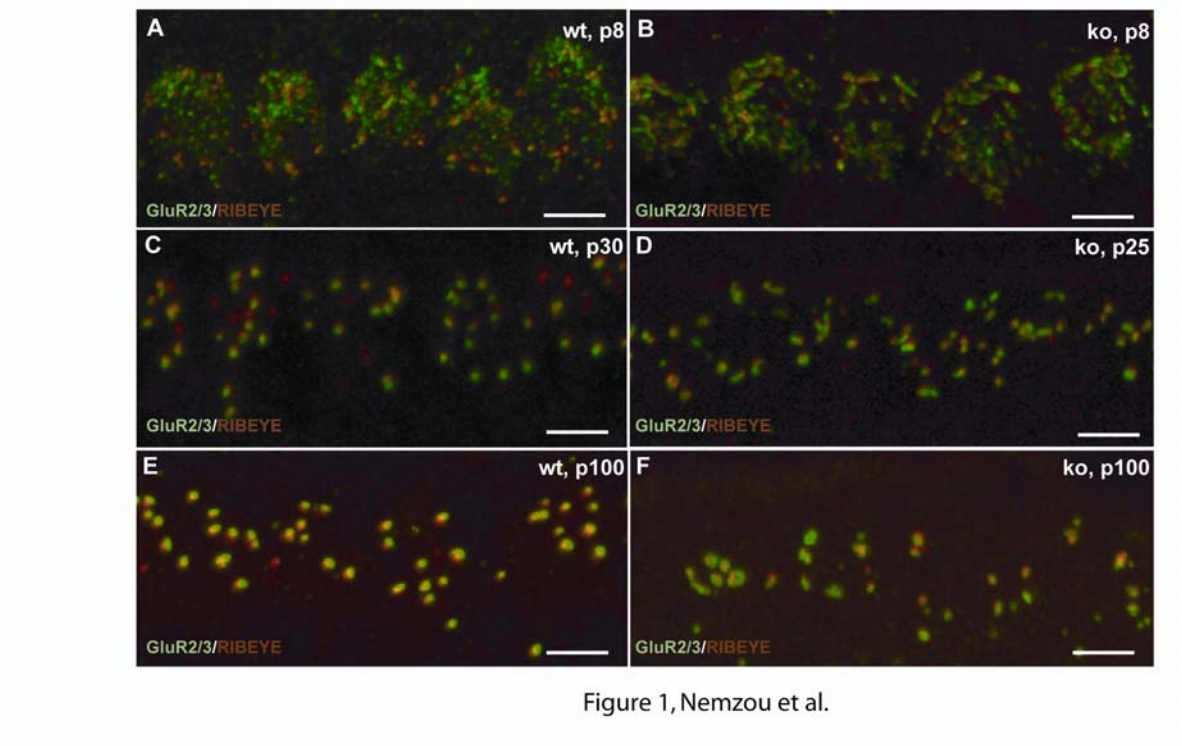

Figure 1. Intact afferent synapse formation and slow loss of ribbon synapses in $Ca_V1.3$ deficient IHCs

(A, B) show representative projections of confocal sections obtained from p8 control (A) and $Ca_V1.3$ deficient (B) organs of Corti stained for GluR2/3 (green) and RIBEYE/CtBP2 (red). Synaptic ribbons were identified as small RIBEYE positive spots underneath the IHC nuclei usually juxtaposing GluR2/3 immunofluorescence spots. The abundance and synapse-anchorage of ribbons was comparable between both genotypes. For quantification see Table 2 and Experimental Procedures. (C, D) show representative control (C) and $Ca_V1.3$ deficient (D) organs of Corti from 4-week-old mice following the same staining as in (A). (E, F) same analysis for 3.5–month-old mice illustrating the lower number of ribbon synapses in the $Ca_V1.3$ deficient IHCs. The tissue was ethanol fixed for all panels.

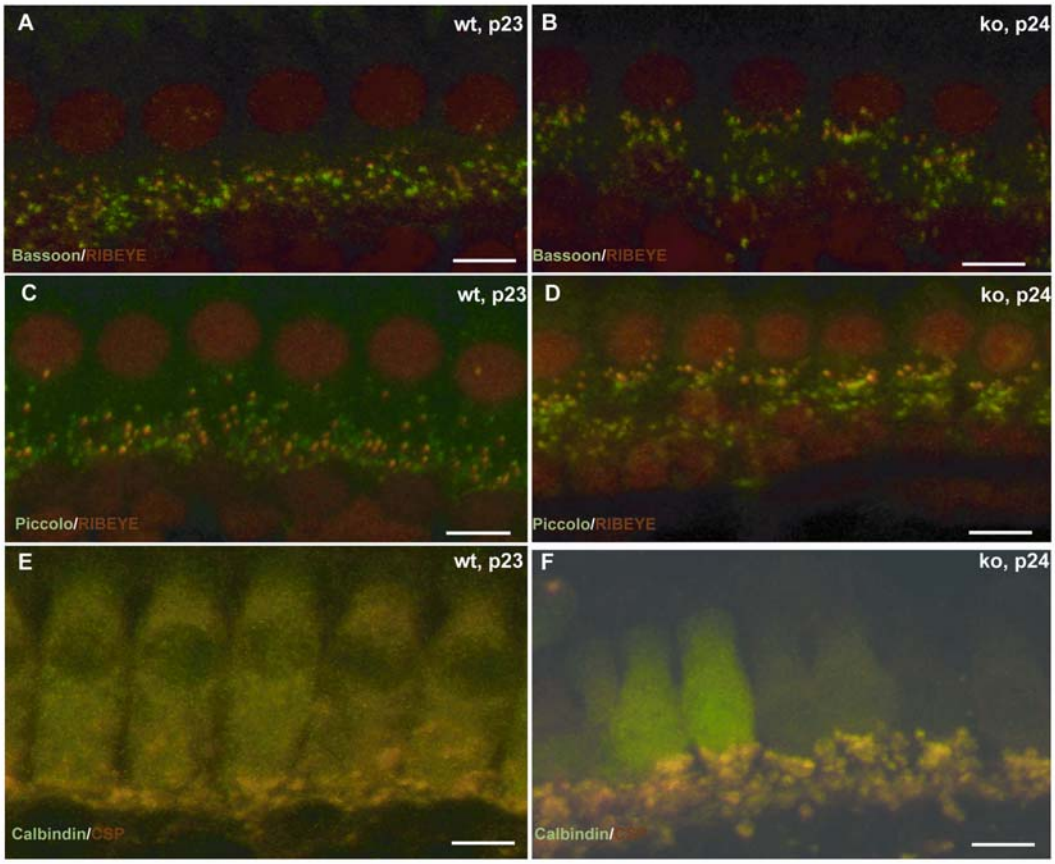

Figure 2, Nemzou et al.

Figure 2. Abundance of key synaptic proteins in $Ca_V1.3$ deficient IHCs

(A, B) show representative projections of confocal sections obtained from 3-week-old control (A) and $Ca_V1.3$ deficient (B) organs of Corti stained for Bassoon (green) and RIBEYE/CtBP2 (red). In both genotypes some of the Bassoon immunoreactive spots partially co-localized with the ribbons marking the hair cell active zones, while other spots did not (most likely efferent presynaptic terminals, Khimich et al. 2005). (C, D) organs of Corti from 3-week-old control (C) and $Ca_V1.3$ deficient (D) mice stained for

Piccolo (green) and RIBEYE/CtBP2 (red). As described before staining for Piccolo results in a similar fluorescence pattern as Bassoon-staining on the light microscopical level in the organ of Corti (Khimich et al., 2005). No differences were observed between the two genotypes, except for the staining in the mutant seemed to be closer to the nucleus. (E, F) staining for the Ca^{2+} buffer protein Calbindin (green) and CSP (red) in organs of Corti from 3-week-old control (E) and $Ca_V1.3$ deficient (F) mice. CSP immunoreactivity was observed in IHC cytosol and efferent presynaptic terminals near base of the IHCs in both genotypes but slightly reduced in the $Ca_V1.3$ deficient IHCs.

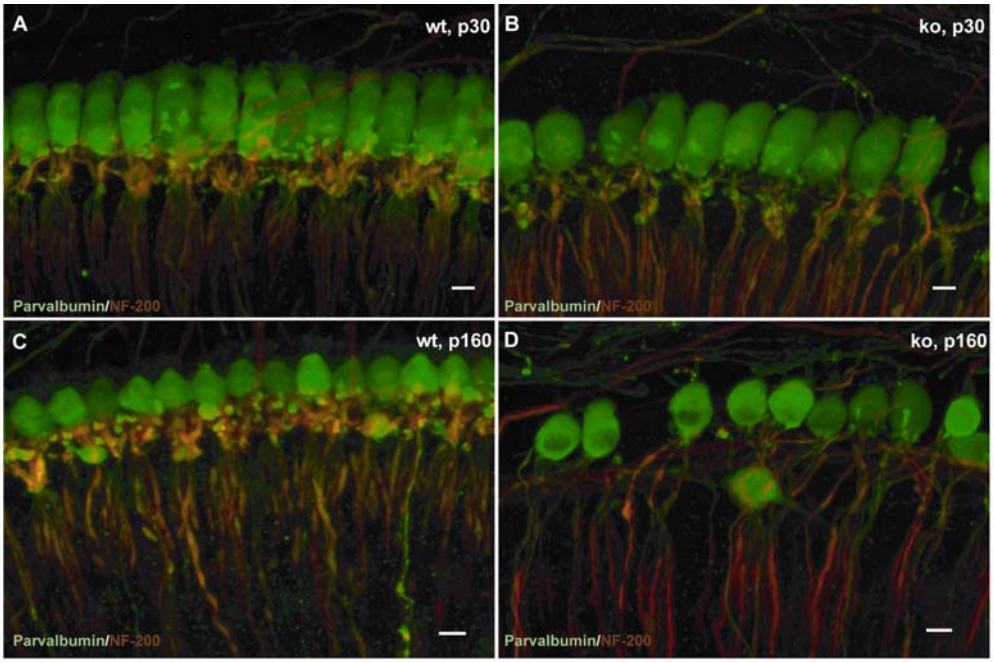

Figure 3, Nemzou et al.

Figure 3 Progressive loss of afferent dendrites in $Ca_V1.3$ deficient mice with age

(A, B) show representative projections of confocal sections obtained from 4-week-old control (A) and $Ca_V1.3$ deficient (B) organs of Corti stained for parvalbumin (green, staining inner hair cells and fibers) and NF-200 (red, fibers) showing comparable number of afferent dendrites in both genotypes at this age. (C, D) demonstrate the reduced number of afferent dendrites and partial loss of IHCs in 5-month-old $Ca_V1.3$ deficient mice (D) in comparison to the control animals of the same age (C). Tissue stained as in (A).

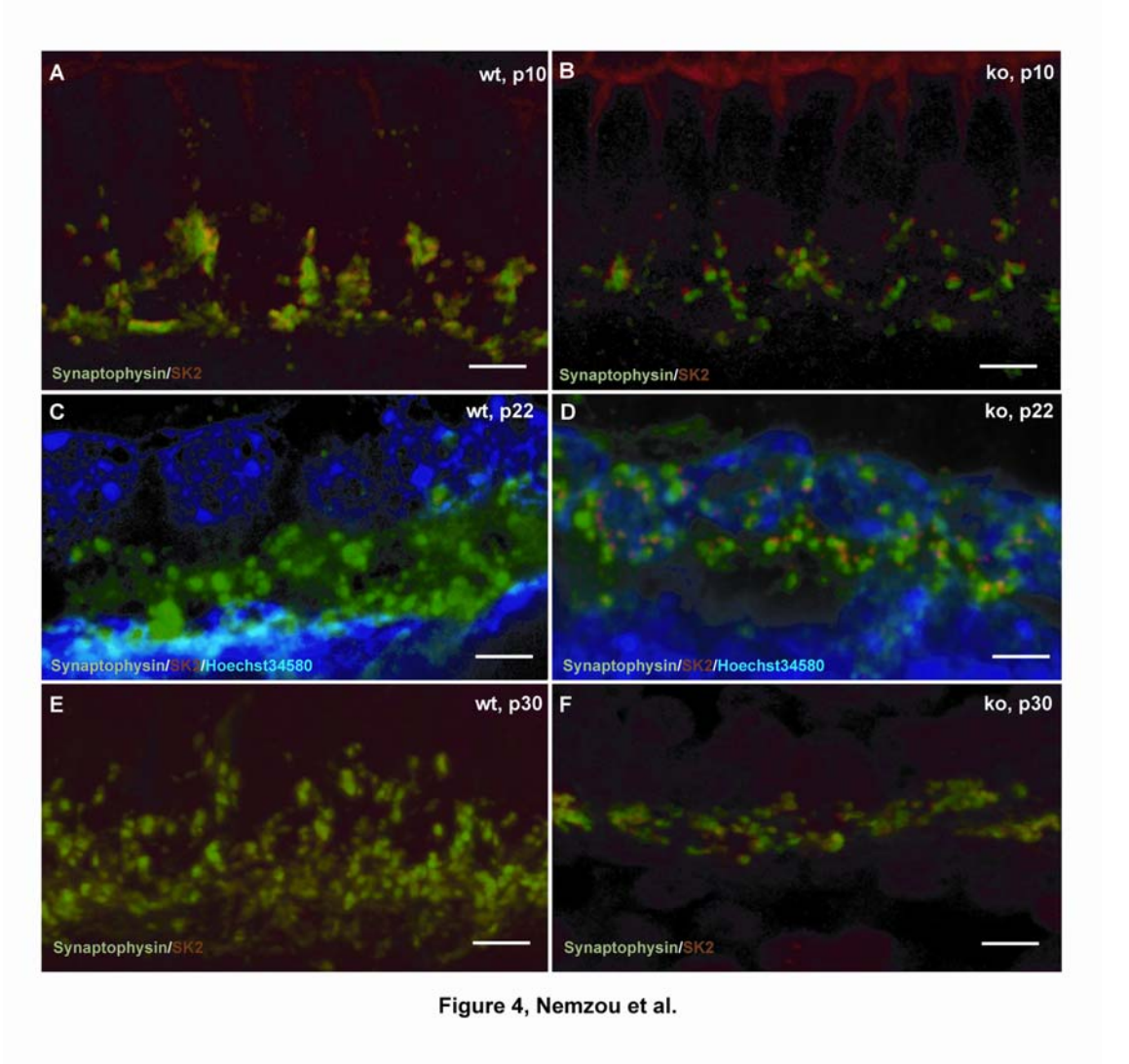

Figure 4 Prolonged presence of efferent axosomatic synapses in $Ca_V1.3$ deficient mice

(A, B) show representative projections of confocal sections obtained from an organ of Corti of control (A) and $Ca_V1.3$ deficient (B) mice on p10 after synaptophysin (green) and SK2 (red) immunostaining. The number of red SK2 spots, juxtaposed to synaptophysin immunofluorescence was counted and related to the number of hair cells in these stretches of the organ of Corti and comparable between the genotypes. (C, D) representative examples obtained from 3-week-old control (C) and $Ca_V1.3$ deficient (D)

mice immunolabeled after methanol fixation and co-stained with the nuclear marker Hoechst 34580 to allow better identification of hair cell position (large blue circular structures). While the mutant IHCs still display a SK2-immunospots (indicating axosomatic synapses), no SK2 immunoreactivity was observed in wildtype IHCs at this age. (E, F) representative examples obtained from 4-week-old control (E) and $Ca_V1.3$ deficient (F) mice stained as in (A) and (B). The mutant IHCs still show some axosomatic synapses even at p30.

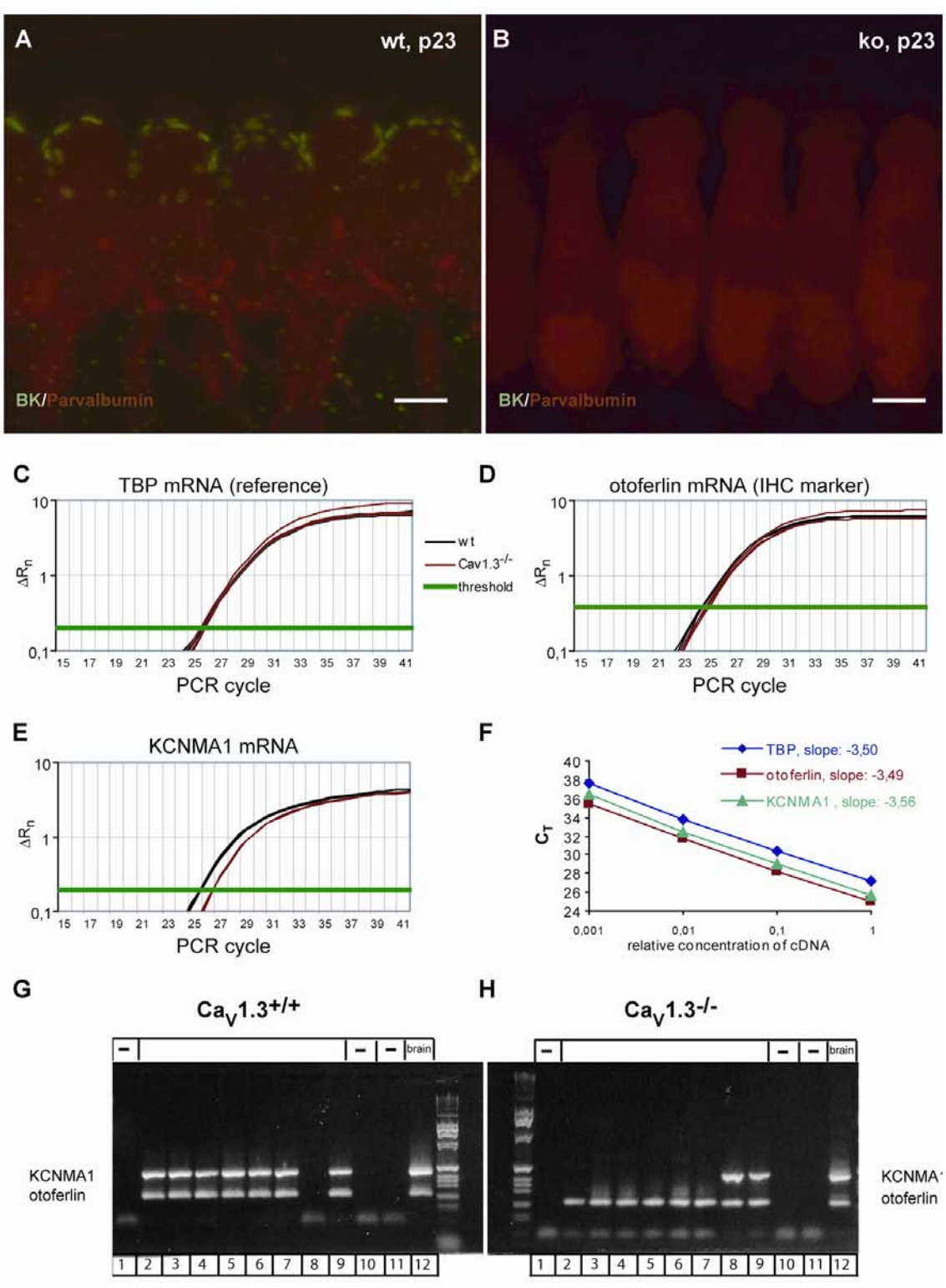

Figure 5, Nemzou et al

Figure 5 Reduced abundance of KCNMA1 mRNA and lack of plasma membrane BK channel immunoreactivity in $Ca_V1.3$ deficient IHCs

(A, B) show representative projections of confocal sections obtained from organs of Corti of control (A) and $Ca_V1.3$ deficient (B) mice of the fourth postnatal week after KCNMA1 (green) and parvalbumin (red) immunostaining: spots of KCNMA1 immunofluorescence at the neck of control IHCs, absence of spots from $Ca_V1.3$ deficient IHCs. (C) real-time PCR of cDNA for the reference TBP. Total RNA was obtained from 8 apical cochlear turns of control and $Ca_V1.3$ deficient mice at p28 and p26, respectively**.** Figure shows a semi-logarithmic plot of amplification curves (relative fluorescence changes [ΔR_n] vs. cycle number, in triplicates) obtained on cDNA from wild-type and knockout animals, which largely overlap. Cyan line indicates threshold, as determined by the cylcer's software. The mean C_T values amounted to 26.0 ($Ca_V1.3^{+/+}$) and 26.1 ($Ca_V1.3^{-/-}$). (D) real-time PCR of cDNA for the IHC marker otoferlin run on cDNA of the same sample as for (C). Amplification curves obtained on cDNA from $Ca_V1.3$ deficient mice are slightly right-shifted with respect to control, indicating a slightly reduced abundance of otoferlin mRNA in mutants. Mean C_T values amounted to 24.8 ($Ca_V1.3^{+/+}$) and 25.1 ($Ca_V1.3^{-/-}$). (E) real-time PCR for KCNMA1 run on cDNA of the same sample as for (C). Amplification curves obtained on cDNA from $Ca_V1.3$ deficient mice are right-shifted with respect to control, indicating a decreased amount of KCNMA1 mRNA in mutants with mean C_T values of 25.9 ($Ca_V1.3^{+/+}$) and 26.9 ($Ca_V1.3^{-/-}$). (F) real-time RT-PCR standard curves for TBP, otoferlin and KCNMA1 cDNA of the same sample as in C ($Ca_V1.3^{+/+}$ only). Mean C_T values are plotted versus different dilutions on a logarithmic scale. Lines represent linear fits to the data yielding the slopes provided in the figure. (G,

H) representative gels showing the products of the nested RT-PCR reaction of 8 individual IHCs from $Ca_V1.3^{+/+}$ (G) or $Ca_V1.3^{-/-}$ (H) mice for KCNMA1 mRNA (upper band) and otoferlin mRNA (lower band) along with negative controls (-) and positive controls (brain). Lane No. 8 of $Ca_V1.3^{+/+}$ was negative for both otoferlin and KCNMA1 mRNAs. (G, H) demonstrate the reduction in the number of IHCs with detectable amount of KCNMA1 mRNA in $Ca_V1.3^{-/-}$ mice.

Table1 Otoferlin and KCNMA1 specific primers used for single IHC RT-PCR

	Forward primer 5'-3'	Reverse primer 5'-3'
otoferlin	GCAGAAGAGCAGCTATGAGC	TCTCCACAGCTAGTCCCAAC
otoferlin nested	AGACTTGTTCCCCCCACTC	TTCATTCAAGTCCTGGTGCTC
KCNMA1	CCAGACACTGACTGGCAGAGTCC	GGGACGTAGCTGGCAAACATGGCC
KCNMA1 nested	ACATGGCTTTCAACGTGTTCTTCC	AAACGTCCCCATAACCCACTGTAG

Table 2 Quantification of the immunohistochemical findings obtained in IHCs of control and $Ca_V1.3$ deficient mice at different ages.

The numbers of immunostained synaptic ribbons (total number of ribbons), ribbons juxtaposing postsynaptic GluR2/3 clusters (ribbon-containing synapses), postsynaptic SK2 immunofluorescent spots juxtaposing presynaptic synaptophysin spots (number of SK2 spots) and projections to IHCs (number of projections to IHC) were quantified in 3D reconstructions of the organ of Corti from confocal sections. For counting the 3D reconstructions were rotated and previously considered regions were successively occluded. These estimates were related to the number of IHCs in the field of view, yielding a count per IHCs. Data are presented as mean ± sem, n represents the number of cochlear regions investigated by confocal microscopy for a given age and analysis.

Superscript P and E indicate fixation by paraformaldehyde and ethanol (see Experimental Procedures).

Age (days)	**8-10**	**12**	**25-30**	**45**	**55-65**	**90-110**	**160-180**	**200**	
Number of ribbon-containing synapses per IHC		15.9±0.2 (n=6)^{E} 15.3±0.2 (n=6)^{E}	10.6±0.2 (n=8)^{E} 9.7±0.9 (n=6)^{E}	n.d. n.d.	10.4±0.2 (n=5)^{E} 4.9±0.1 (n=6)^{E}	10.5±0.1 (n=6)^{E} 3.6±0.3 (n=6)^{E}	10.1±0.2 (n=5)^{E} n.d.	9.9±0.2 (n=5)^{E} 2.1±0.1 (n=6)^{E}	**wt** **ko**
Total number of ribbons per IHC	18.7±0.3 (n=6)^{E} 19.6±0.3 (n=5)^{E}	n.d. n.d.	11.7±0.1 (n=5)^{P} 10.5±0.2 (n=6)^{P}	n.d. n.d.	11.4±0.1 (n=5)^{P} 5.3 ±0.3 (n=5)^{P}	11.0±0.2 (n=5)^{P}	10.3±0.2 (n=6)^{P} 3.6±0.2 (n=7)^{P}	10.3±0.2 (n=4)^{E} 2.8±0.1 (n=5)^{P}	**wt** **ko**
Number of dendrites fibers per IHC	n.d. n.d.	10.0±0.0 (n=6)^{P} 7.2±0.2 (n=6)^{P}	9.9±0.1 (n=6)^{P} 7.7±0.4 (n=7)^{P}	n.d. n.d.	10.0±0.1 (n=6)^{P} 5.3±0.4 (n=5)^{P}	9.7±0.2 (n=7)^{P} 5.6±0.8 (n=6)^{P}	10.5±0.4 (n=6)^{P} 4.7±0.2 (n=6)^{P}	10.3±0.1 (n=6)^{P} 4.1±0.4 (n=6)^{P}	**wt** **ko**
SK2-spots per IHC	18.6±0.3 (n=5)^{P} 11.5±0.3 (n=5)^{P}	n.d n.d.	0 (n=5)^{P} 6.5 ±0.5 (n=5)^{P}	0 (n=5)^{P} 1.9±0.3 (n=5)^{P}	n.d. n.d.	n.d. n.d.	n.d. n.d.	n.d. n.d.	**wt** **ko**